Mechanistic study of heterogeneous propene metathesis on WO_x/SiO_2 catalysts

Anne V. Le,[a,c] *Biplab Rajbanshi,*[a,c,1] *Raul F. Lobo,*[b,c] *Peng Bai* [a,c,*]

[a]Department of Chemical Engineering, University of Massachusetts Amherst, Amherst, MA 01003-9303, United States

[b]Department of Chemical and Biomolecular Engineering, University of Delaware, Newark, DE 19716, United States

[c]Center for Plastics Innovation, University of Delaware, Newark, DE 19716, United States

[*]Corresponding Author: pengbai@umass.edu

[1] Current address: Department of Chemistry, Visva-Bharati University, Santiniketan 731235, Birbhum, West Bengal, India

KEYWORDS: olefin metathesis • silica-supported tungsten oxides • heterogeneous catalysis

ABSTRACT: Silica-supported tungsten oxides are widely used industrial catalysts for olefin metathesis due to their low cost and robustness, yet the mechanisms for heterogeneously catalyzed metathesis reactions remain comparatively less understood. In this work, density-functional theory (DFT) calculations were used to study the model reactions of propene metathesis. Our calculations confirm that the metathesis reactions catalyzed by WO_x/SiO_2 largely follow the Chauvin cycle, with an overall energetic barrier of 142 kJ/mol. To understand how the initial alkylidene active sites are generated, three mechanisms were examined: The pseudo-Wittig mechanism was found to be most favorable and proceeds with a metallacycle intermediate, while the allylic and vinylic C-H activations are much more difficult and require the reduction of surface sites to W(+4). Relative to the adsorbed reactant state, the overall intrinsic barriers for three mechanisms were computed to be 193, 261, and 355 kJ/mol, respectively. The higher barriers for active-site formation than for the metathesis cycle are consistent with the difficult, high-temperature pretreatment required in experiments to activate WO_x/SiO_2 catalysts.

Introduction

Olefin metathesis, an organic reaction involving the cleavage and reassembling of C=C double bonds, plays an important role in the chemical industry. Coupled with alkane dehydrogenation, this reaction provides a powerful potential route for deconstructing long-chain saturated hydrocarbons to make fuel- and lubricant-range products.[1,2] In this context, the reactions are termed molecular weight averaging and redistribution[3] and have been explored as a method for polyolefin upcycling.[2] Olefin metathesis was first developed as a heterogeneous process[4] and saw significant development in the homogeneous context during the 1960s and 1970s. Many active catalyst systems have been developed and the mechanism proposed by Chauvin[5,6] has been accepted for homogeneous metathesis with alkylidene carbenes as the active center that undergoes [2+2] cyclo-addition and cyclo-reversion. By contrast, the characterization of the metallacycle intermediates encountered in heterogeneous catalysis appeared some twenty years later, in the mid-1980s.[7] A mechanistic picture for heterogeneous metathesis reactions, especially with respect to the generation and nature of the active sites, is much less clear.[8]

The catalysts used most often in heterogeneous olefin metathesis include the oxides of molybdenum, tungsten, and rhenium supported on alumina, silica, or their mixtures. Given the difficulty of observing the active species on these catalysts directly, much information has been gleaned using surface organometallic chemistry approaches or from studies on molecularly defined clusters.[7,9,10] For example, Bouhoute et al. sought to confirm the hypothesized bipodal, mono-oxo W(VI) carbene active sites by synthesizing a tungsten species $(\equiv SiO)_2WO(CH_2SiMe_3)_2$ and demonstrating that these species can convert to active mono-oxo tungsten catalysts for propene metathesis.[11] Mougel et al. similarly prepared molecularly defined, isolated W(VI) oxo sites on silica, which, after treatment with organosilicon reductants, became active for metathesis at 70 °C.[12] Based on XANES and EPR spectra, the authors suggested that active sites are formed from W(IV) species through an oxidative pathway to generate W(VI) carbenes. Using solid state NMR, Blanc et al. attempted to directly observe the metallacyclobutane intermediate and alkylidene species; here, the authors were able to corroborate previous findings correlating the high stability of an intermediate with square-pyramid geometry (SP) with low reactivity while associating the alternative trigonal bipyramid geometry (TBP) with high reactivity. [13] These results demonstrated that tungsten alkylidenes can be active towards olefin metathesis and metallacyclobutanes are important intermediates, both of which can be tuned through functionalization at the tungsten site.

Theoretical studies have also revealed mechanistic insights on the initiating reactions that produce the alkylidene active sites and provided geometrical analysis on the stability of mono- and dioxo species. For example, Handzlik et al. used density-functional theory (DFT) calculations and found that the most favorable molybdenum and tungsten oxide structures depend on local silica support geometry and that the silanol groups on the silica surface can facilitate the reduction of the molybdenum center to generate the alkylidene active site through an alkoxy species.[14–16] Regarding the stability of mono- and dioxo species, the authors showed that dioxo Mo(VI) is more favored as the pre-active site species compared to mono-oxo Mo(V) as their activation barriers differ by 30 – 40 kJ/mol, but this gap closes at $T = 823$ K to only 3 – 8 kJ/mol.[14]

Despite these advancements, questions regarding which active-site formation mechanism dominates on a particular catalyst and how to increase active site concentration remain. For example, Howell et al.[17] found that on tungsten oxides, consistent with previous reports,[18] the steady-state TOF increases with increased tungsten surface coverage up to the nanoparticle formation limit, suggesting that only isolated tungsten sites are potential active species. They also observed that He pretreatment doubles TOF compared to air-pretreated catalysts. With the latter, acetone forms at the onset of reaction and decays with a time constant closely aligned to the time constant for the increase in metathesis activity. The authors suggested that the observed acetone is a consequence of reducing $W(VI)O_2$ to W(IV)O, and integration of the acetone formation for a sample containing 0.6 W/nm^2 indicated that only 5% of tungsten was converted to an active site. Other oxygenates such as acetaldehyde have also been experimentally observed.[18,19] Wachs et al. carefully studied the activation of supported WO_x/SiO_2 catalysts.[18,20] Their in-situ XANES analysis showed that dioxo WO_4 sites were the dominant surface sites[18] and they found that the number and reactivity of activated surface WO_x sites increase with activation temperature, olefin partial pressure, and olefin size.[20] Gani et al. reported an interesting approach to operate an active site decay/renewal cycle in parallel with the Chauvin metathesis cycle. The active-site renewal was promoted by proton transfers involving neighboring acidic OH groups on silica surface and co-feeding olefins such as 2,3-dimethyl-1-butene (i4ME) that are known to not undergo cross-metathesis.[21] These studies pointed to the importance of catalysts activation, the detrimental effects of oxygenates, and the role different olefins may play in maintaining the activity of activated tungsten sites.

In this work, we present results from ab-initio DFT calculations for WO_x/SiO_2 catalyzed metathesis cycle, various initiating mechanisms, and two pathways for the reduction of W(VI) sites. The initiating mechanisms studied include the pseudo-Wittig, allylic, and vinylic pathways.[7,8,22] For the interconversion of tungsten oxides from the highest oxidation state of WO_2(VI) to the reduced state WO(IV), both H_2 and propene were considered as the potential reductant. We report the energetic barriers and transition-state structures for each mechanism to identify the dominant pathways and elucidate structural factors that influence reactivity.

Methods

The reaction pathways for alkylidene generation and propene metathesis were studied on an isolated tungsten site sitting on top of a seven-membered siloxane ring of a silica support. The model structure was taken to be the most likely site based on the work of Kurleto el al[15] and was a partially dehydroxylated variant of an amorphous SiO_2 slab model initially proposed by Tielens et al.[23] The silica support consists of 27 Si atoms and a vacuum layer of 15 Å was then added, resulting in a simulation cell of dimensions 12.77 × 17.64 × 25.17 $Å^3$. Periodic DFT calculations were performed using the Vienna Ab initio Simulation Package, version 6.1.2,[24,25] with the PBE exchange-correlation functional[26] and Grimme-type D3 dispersion corrections with the Becke-Johnson damping.[27,28] Valence electrons were expanded using a plane-wave basis set with a kinetic energy cutoff of 400 eV while the core electrons were treated using the projector augmented wave (PAW) method.[25,29] The PAW potentials used include 4 (C), 6 (O), 4 (Si), and 6 (W) valence electrons. Sampling of the Brillouin zone was done at the Γ point only. All calculations were non-spin polarized, as tests for WO(IV) with spin polarization and with initial atomic magnetic moments set to high values converged reliably to a clean singlet state. The geometries for all reactants, products, and stable intermediates were optimized with a force criterion of 0.05 eV/Å.

To search for transition states, nudged elastic band (NEB)[30] calculations using 8 – 16 images were performed first to a convergence criterion of 10^{-5} eV/Å, which were followed by the climbing-image NEB variant[31] using 32 images and a convergence criterion of 10^{-6} eV/Å. As an additional verification, vibrational analysis was conducted for all transition-state structures for all atoms within a radius of 7 Å of tungsten. As shown in Supplementary Table S5, a dominant negative eigenmode was found in all cases, along with 1 – 3 additional negative modes of small magnitudes that were not able to fully optimize away at the resolution of the NEB calculations. The first negative eigenmodes for all reaction pathways were visualized to make sure that they correspond to the reaction transitions of interest. The visual inspection also revealed that the extraneous negative modes correspond to surface hydroxy and framework torsions. The many low-frequency modes are characteristics of computing complex reactions with a large model system, which makes the standard harmonic-oscillator treatment highly unreliable. In addition, more

important contributions to entropy and free energy for these complex reactions may arise from other configurations in the reactant basin or on the transition-state dividing surface, including different conformations on a single site and equivalent transitions on other sites, rather than small harmonic deviations from the stationary points. Proper ensemble-averaged kinetic parameters will thus be a balance between the active-site populations and the reactivity of each site.[32,33] Since this work focuses on the systematic evaluation of mechanisms by studying only the most likely tungsten site, we decided to report only energy profiles, which in our opinion are well defined without the intrusion of unquantifiable errors.

Results and Discussions

Interconversion of W(VI) active-site precursors

Geometry optimizations and transition-state searches were performed to characterize the stability of the species involved in the overall catalytic cycle for propene metathesis on WO_x/SiO_2 catalysts as shown in **Scheme 1**. This mechanistic picture is constructed based on the postulated di-grafted tungsten oxo alkylidene species as the active site (**C_0**) and includes the assumed interconversion between its pre-active forms (**A_0**, **A_1**, and **A_4**). Among these, **A_1** is a tetra-grafted, mono-oxo tungsten site, which can convert to **A_0**, di-grafted, di-oxo tungsten, through the hydrolytic cleavage of two of the four W-O bonds. Therefore, one mono-oxo tungsten site can produce four different di-oxo tungsten forms. Kurleto et al. examined two mono-oxo and eight di-oxo WO_x models and observed a significant effect of the site location, which led to a difference of > 250 kJ/mol between the two mono-oxo models.[15] For the more stable mono-oxo model, its corresponding set of four di-oxo forms can further differ in energy by 1–35 kJ/mol. Based on their study, we focus on the most favorable di-oxo and mono-oxo models in our subsequent calculations. The two chosen WO_x models are distinguished by the supporting 7-membered siloxane ring, whereas the other less stable models have 2-, 3-, and 4-membered siloxane rings.[15] As shown in **Figure 4**, the bipodal, di-oxo W(VI) species, **A_0**, has a tetrahedral geometry, with an O=W=O angle of 108°. The bond lengths between W and the two oxo ligands are identical, at 1.73 Å, similar to the values of 1.70 – 1.73 Å reported by Kiani et al.[34] The bond lengths between W and the two surface oxygen atoms are also similar, at 1.87 and 1.90 Å, compared to 1.89 – 1.93 Å from the same study.[34]

Scheme 1. Schematics of active-site formation mechanisms and the metathesis cycle on supported WOx/SiO_2 catalysts: (a) the pseudo-Wittig pathway for generating methylidene active sites, (b) metathesis cycle, (c) reduction of W(VI) sites by H_2, involving a Si-O-W group from the silica support or the metal center, (d) the allylic pathway for generating a methylidene active site, where the allylic hydrogen migrates through the metal center as a hydride or the oxo-ligand as a proton, and (e) the vinylic pathway for generating a propylidene active site.

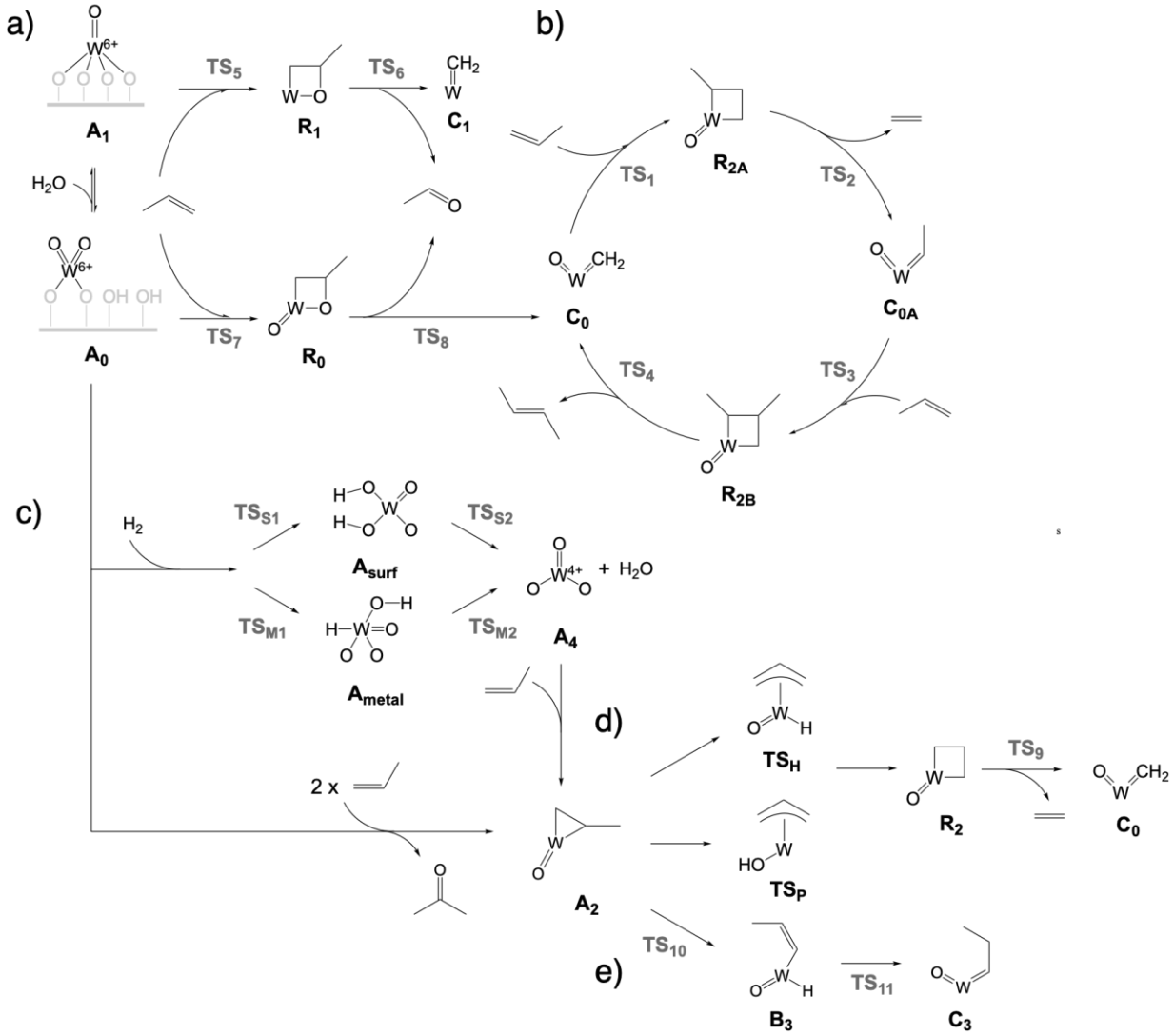

Our calculations found no energy change for the conversion of $\mathbf{A_1} \rightarrow \mathbf{A_0}$, compared to the very small increase of 4 kJ/mol reported by Kurleto et al.,[15] who also observed that the reaction energy could further increase to 38 kJ/mol depending on the choice of which two W-O bonds are broken. In an earlier work, Howell et al. studied an analogous conversion of tungsten sites that are supported on a 4-membered siloxane ring and found a reaction energy of −41 kJ/mol.[17] In all cases, however, as pointed out by Howell et al., the hydrolysis reaction involving gas-phase water molecules comes with a significant loss of translational entropy and the di-oxo species therefore exhibit higher free energies at the high-temperature

reaction conditions for metathesis. On the other hand, comparison of computational results and experiments suggests di-oxo tungsten as the majority species,[15,35] especially with He pretreatment,[17] which is likely due to the limited availability of large siloxane rings that can support tetra-grafted, mono-oxo species compared to the more geometrically unrestricted di-oxo species.[15]

Metathesis cycle catalyzed by supported WO_x/SiO_2 catalysts

Energies for the different elementary steps of the metathesis cycle, assuming gas-phase reactants and products, are illustrated in **Figure 1**. The heterogeneous metathesis cycle is hypothesized to follow the well-known homogenous Chauvin mechanism consisting of repeated [2+2] cycloaddition and retro-[2+2] cycloreversion steps with metallacycle intermediates (**R_{2A}** and **R_{2B}**). The cycle starts with propene coordination to the methylidene active site (**C_0**) via [2+2]-cycloaddition, a relatively easy step with an activation energy of 11 kJ/mol that produces a stable metallacyclobutane (**R_{2A}**, −102 kJ/mol). Next, this ring intermediate undergoes cycloreversion with an activation energy of 141 kJ/mol, which generates ethylidene (**C_{0A}"**) and ethene. **Figure 1** further assumes the desorption of ethene and adsorption of a second propene molecule, which leads to **C_{0A}'** and **C_{0A}**, respectively. Both are similar in energy to the methylidene species, differing by 4 or −1 kJ/mol compared to **C_0'** and **C_0**. The ethylidene undergoes another cycloaddition step with an activation energy of 58 kJ/mol to give the di-methyl metallacyclobutane (**R_{2B}**, −103 kJ/mol). Finally, cycloreversion on this ring structure ($\Delta E^{\neq}$ = 97 kJ/mol) releases 2-butene and completes the catalytic cycle.

Overall, the self-metathesis of propene to produce ethene and 2-butene is nearly thermo-neutral, with a reaction energy of 3 kJ/mol, which is comparable with the value of 8.8 kJ/mol, calculated using the experimental heats of formation from the NIST Webbook.[36] The overall activation barrier was obtained as the largest energy span from the transition state for the first cycloreversion step, **TS_2**, to the metallacycle intermediates **R_{2B}**, at 142 kJ/mol. This value is consistent with the relative high operating temperatures required experimentally (e.g., 573 – 693 K).[2,17] Experimental studies have reported a wide range of activation barriers,[17,37,20] which seems to depend on the type of tungsten active sites and can range from 100 to 300 kJ/mol.[20]

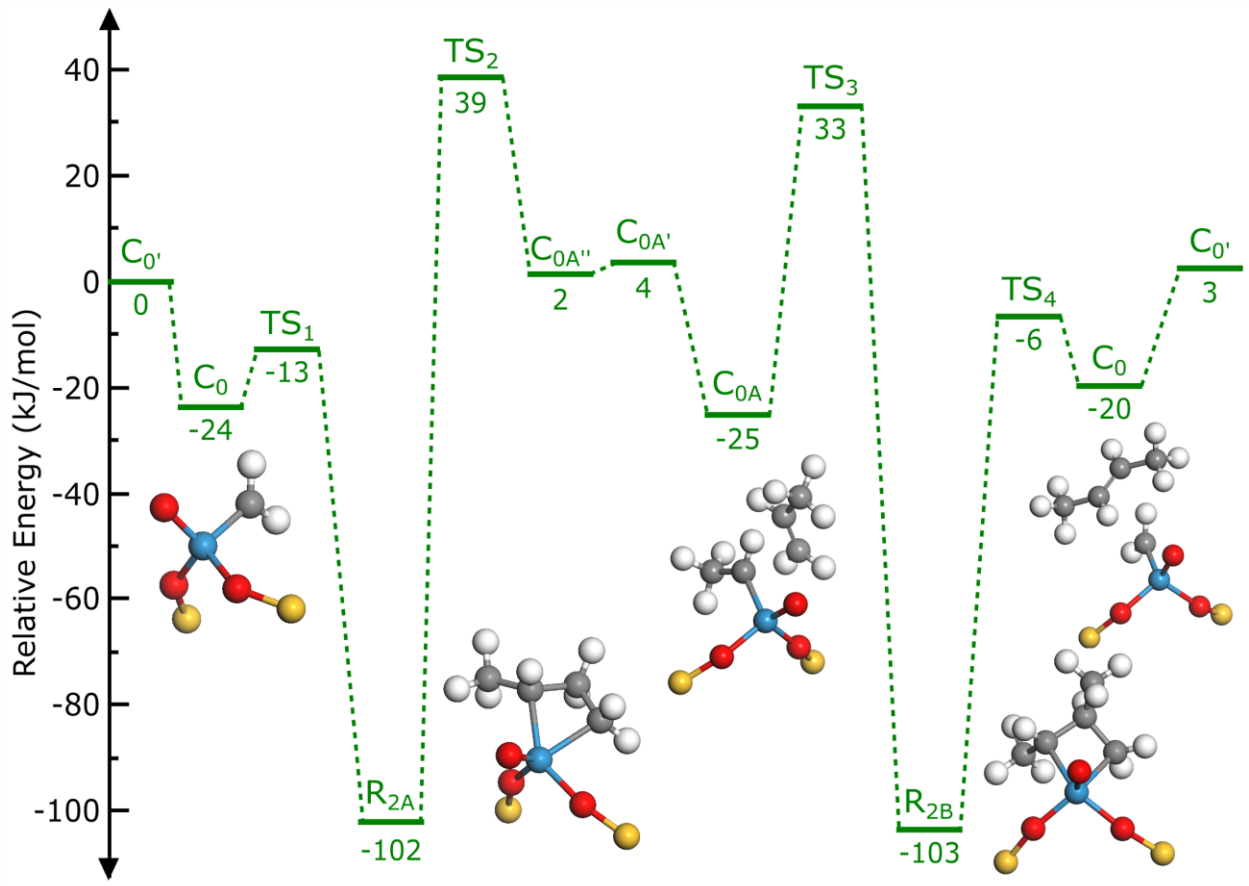

Figure 1. Energy profile for the catalytic cycle of propene metathesis on a di-grafted $(\text{-SiO})_2\text{WO=CH}_2$ methylidene active site, with species labeled according to **Scheme 1b**. **C_0'** and **C_{0A}'** denote the same surface species as **C_0** and **C_{0A}**, respectively, but with propene in the gas phase, while **C_{0A}''** has a physisorbed ethene compared to **C_{0A}'**.

Figure 2 shows optimized structures for intermediates in the metathesis cycle with key bond lengths and bending angles highlighted. The numerical values are listed in Supplementary Table S1. Both the initial oxo-tungsten methylidene (**C_0**) and ethylidene (**C_{0A}**) species exhibit a tetrahedral geometry with very similar structures. The W=O bond lengths are 1.71 and 1.72 Å, while the W=C bond lengths are 1.89 Å and 1.90 Å, respectively. The two tungstacyclobutane intermediates (**R_{2A}** and **R_{2B}**) also share a similar, square-based pyramid (SBP) geometry, with the W=O distance being 1.73 Å and the W-C bond lengths being 2.17 – 2.18 Å. The C-C-C angles are 96 – 97° with the two C-C bond lengths characteristics of those of C-C single bonds, at 1.53 – 1.54 Å. The structures of the ring intermediates have been the subject of several studies. In addition to the SBP geometry, NMR experiments[13] also observed the trigonal

bipyramidal (TBP) geometry, where the metal-bonded carbon atoms and an anionic ligand (e.g., oxygen atom in this work) lie in the same plane. The SBP configuration is generally found to be more stable than the TBP configuration except with bulky anionic ligands.[38,39] The X-ray determined structure of a SBP imido-tungstacyclobutane complex gave distances of 2.14 and 2.17 Å for the W-C bonds and 1.55 and 1.57 Å for the C-C bonds, which agrees well with our results. Similar structural parameters are also reported in the computational work of Solans-Monfort,[39] which found no significant influence of the metal or the ligands on the geometrical features of these metallacycle intermediates. Finally, it is worth noting that the four transition states (TS) are fully equivalent, although obtained for different elementary steps, because they are equivalent saddle points on the potential energy surface connecting the reversible interconversion between alkylidene and metallocyclobutane species. Since the cycloreversion of $\mathbf{R_{2A}}$ can go in either the forward or backward direction, $\mathbf{TS_1}$ can be viewed as the result of either the [2+2] addition of propene to $\mathbf{C_0}$, as described above, or the backward cycloreversion of $\mathbf{R_{2A}}$.

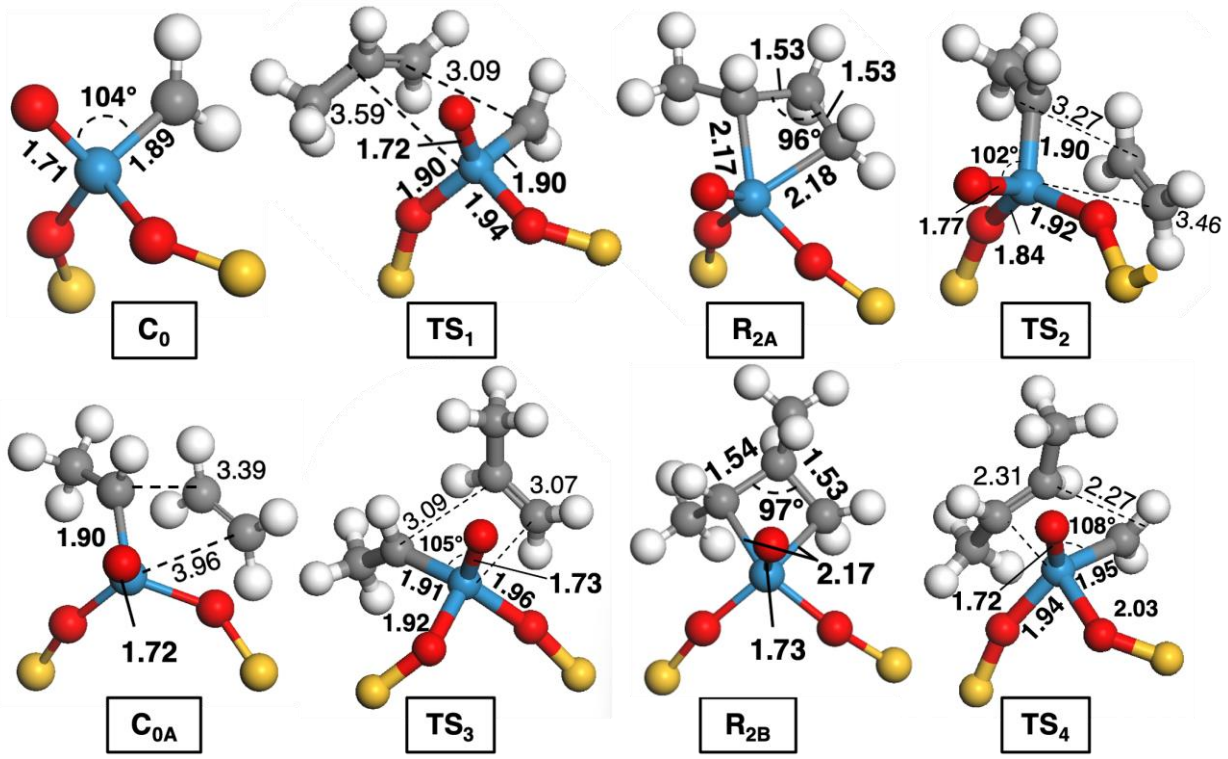

Figure 2. Optimized structures from the heterogeneous metathesis cycle including the alkylidene active site ($\mathbf{C_0}$ and $\mathbf{C_{0A}}$) and metallacycle intermediates ($\mathbf{R_{2A}}$ and $\mathbf{R_{2B}}$). Bonded distances are shown in bold, while non-bonded distances are shown with normal text and dashed lines.

Generation of oxo tungsten alkylidene active sites

For supported heterogeneous metathesis catalysts, a key question concerns the generation of alkylidene active sites from the experimentally observed oxo metal species. Over the years, several mechanisms have been proposed including the pseudo-Wittig mechanism, allylic C-H activation, and vinylic C-H activation (**Scheme 1a**, **d**, and **e**). Among these active-site initiation mechanisms, both C-H activation routes formally involve the reduction of the metal center prior to alkylidene formation, while the pseudo-Wittig mechanism maintains the metal center at an oxidation state of +6 throughout the reaction pathway.

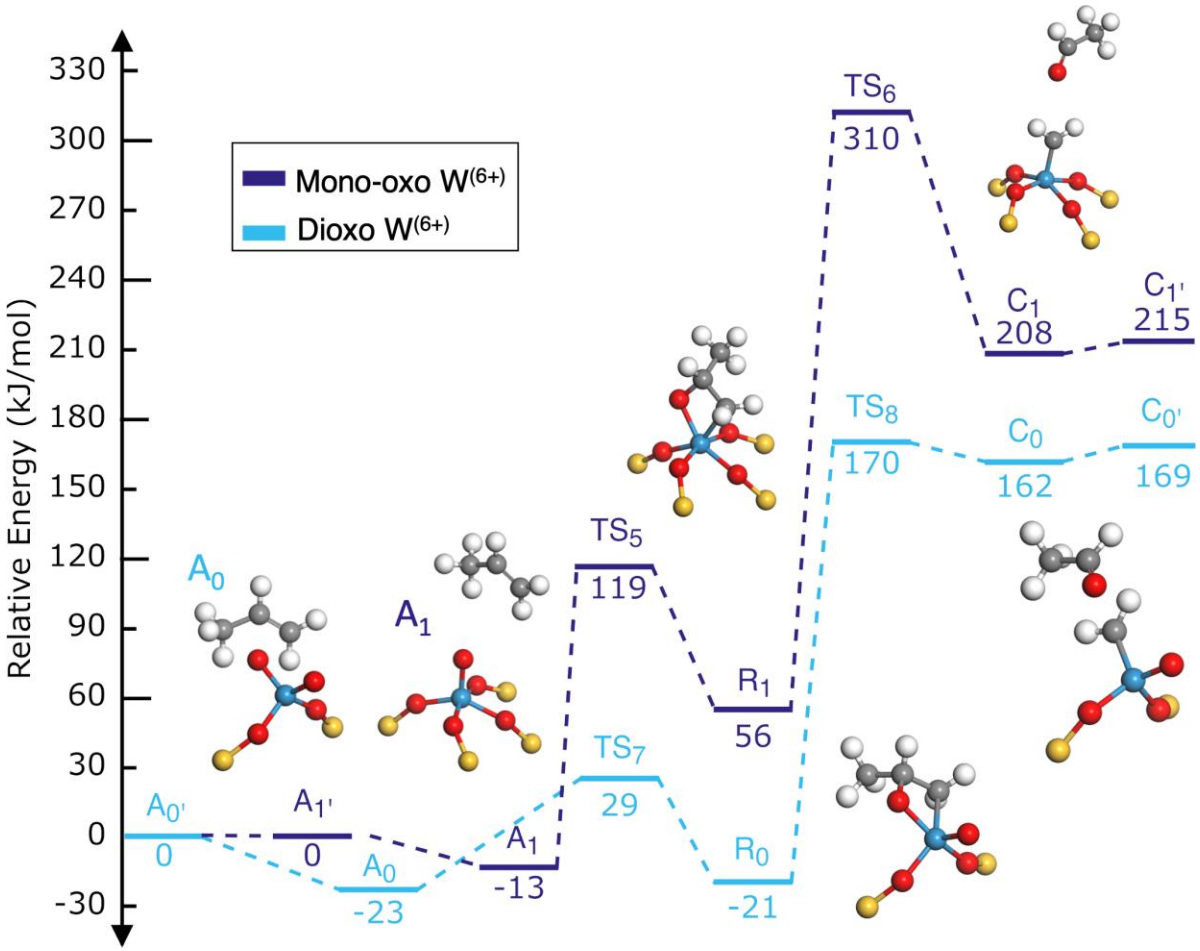

Figure 3. Energy profile for the pseudo-Wittig reactions of $(\text{-SiO})_4\text{WO}$ vs. $(\text{-SiO})_2\text{WO}_2$ in dark blue and cyan, respectively. Primed symbols represent structures with reactants desorbed to the gas phase.

Pseudo-Wittig mechanism

The energy profiles for the pseudo-Wittig mechanism, starting from either the bipodal, di-oxo **A$_0$'**, or the tetra-grafted, mono-oxo **A$_1$'**, tungsten species, are presented in **Figure 3**, and key structural parameters

for intermediates and transition states are shown in **Figure 4** and Supplementary Table S2. The reaction sequence starting from either initial compound is largely similar and resembles the metathesis cycle itself, although with dramatically different energetics. The di-oxo pathway begins with [2+2] cycloaddition of propene to form an oxametallacycle (**R_0**) with a mild activation energy of 52 kJ/mol and a reaction energy of 2 kJ/mol relative to **A_0** with an adsorbed propene molecule, whereas the activation and reaction energies for the corresponding step in the mono-oxo pathway are much higher, 132 and 69 kJ/mol, respectively, relative to **A_1**. The 4-membered rings have a similar geometry as **R_{2A}** and **R_{2B}** from the metathesis cycle, with a C-C-O angle of 98 – 99°, compared to the equivalent apical angles of 96–97° in **R_2**. The W-C bond lengths in **R_0** and **R_1** are also similar to those in **R_2**, all three having values between 2.17 – 2.18 Å. The W-O bonds are shorter with values of 1.90 and 1.93 Å. The bipodal **R_0** species exhibits a square-based pyramid geometry while the tetra-grafted **R_1** species adopts a distorted trigonal prismatic geometry, which might explain the large energy difference between the two pathways. The oxametallacycle then undergoes cycloreversion and generates the methylidene active site and acetaldehyde, **C_0** and **C_1**. The cycloreversion step is significantly more difficult with an activation energy of 191 and 254 kJ/mol for the bipodal and tetra-grafted pathways, respectively. The resulting methylidene species **C_0'** and **C_1'** are 169 and 215 kJ/mol higher in energy compared to the pre-active tungsten sites **A_0'** and **A_1'**. While the elementary steps are largely analogous, the reaction on a tetra-grafted tungsten site has consistently higher barriers and less stable intermediates for both cyclo-addition and reversion steps. The overall activation barriers for the pseudo-Wittig mechanism, estimated from the energy span from the highest points on the energy profiles to most stable states (**$A_0 \rightarrow TS_8$** and **$A_1 \rightarrow TS_6$**), are 193 and 323 kJ/mol, respectively, indicating that the pseudo-Wittig pathway on a bipodal, di-oxo tungsten site is more likely.

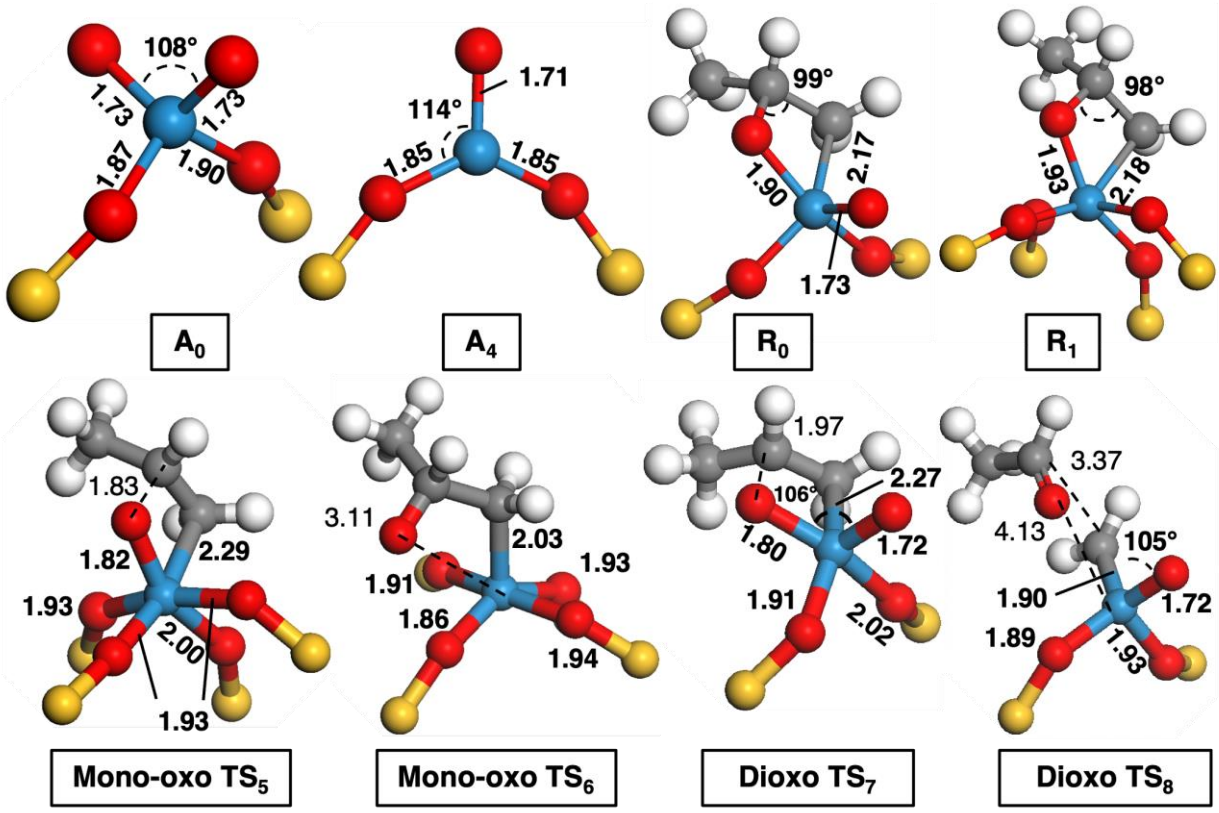

Figure 4. Reactant, intermediate, and transition-state structures for the pseudo-Wittig mechanism and a mono-oxo W(IV) site.

Reduction of supported W(VI) sites

Allylic and vinylic C-H activations are two mechanisms often considered for alkylidene formation. Both mechanisms are usually written for a reduced metal center with open coordination site as the starting compound, such as the bipodal, mono-oxo W(IV) species, shown as **A4** in **Scheme 1c**. The reduction can occur from the corresponding di-oxo W(VI) species during pretreatment and is thought to be critical for improving the catalytic activity.[17] Here, we consider two possibilities with either H_2 or reactant propene as the reductant, the former of which may be produced from the dehydrogenation of alkanes in the case of alkane metathesis.[2] **Figure 5** and **Figure 6** illustrate the energetics and key structures for the H_2-assisted reduction. As shown in **Scheme 1c,** H_2 can undergo either metal-assisted heterolytic cleavage (**A0** → **Ametal** → **A4**) or surface oxygen-assisted homolytic cleavage (**A0** → **Asurf** → **A4**). In the former pathway, H_2 dissociates relatively easily, with an intrinsic barrier of 98 kJ/mol (relative to **A04**), before one of the H atoms migrate from the metal to the hydroxy group to form the transition state, **TSM2**, which features a

fully formed water molecule coordinated to the metal center. In comparison, the surface oxygen-assisted pathway features a transition state with a highly distorted tetrahedral structure, $\mathbf{TS_{S1}}$. The O-W-O angle widens to 111° and the two W-O(H) bonds are elongated to 1.97 and 1.85 Å, compared to the initial dioxo precursor that has an O-W-O angle of 108°, W=O bond lengths of 1.73 Å, and W-O bond lengths of 1.87 and 1.90 Å. **Figure 5** shows that the activation energy relative to $\mathbf{A_{04}}$ (which is $\mathbf{A_0}$' with adsorbed H_2) is 201 kJ/mol for the metal-assisted pathway and 215 kJ/mol for the surface oxygen-assisted pathway. For silica-supported molybdenum, Handzlik et al. reported an analogous effect of surface groups in assisting the formation of alkylidene active site.[15] H_2-assisted reduction of metal sites was also discussed by Salameh et al. with a Re^{7+} complex.[22] In our case, both pathways generate water and the same bipodal, mono-oxo W(+4) species, $\mathbf{A_4}$', which is 189 kJ/mol higher in energy than the corresponding di-oxo W(+6) species. The coordination of propene then forms an oxometallacyclopropane, $\mathbf{A_2}$, the precursor for both allylic and vinylic C-H activations.

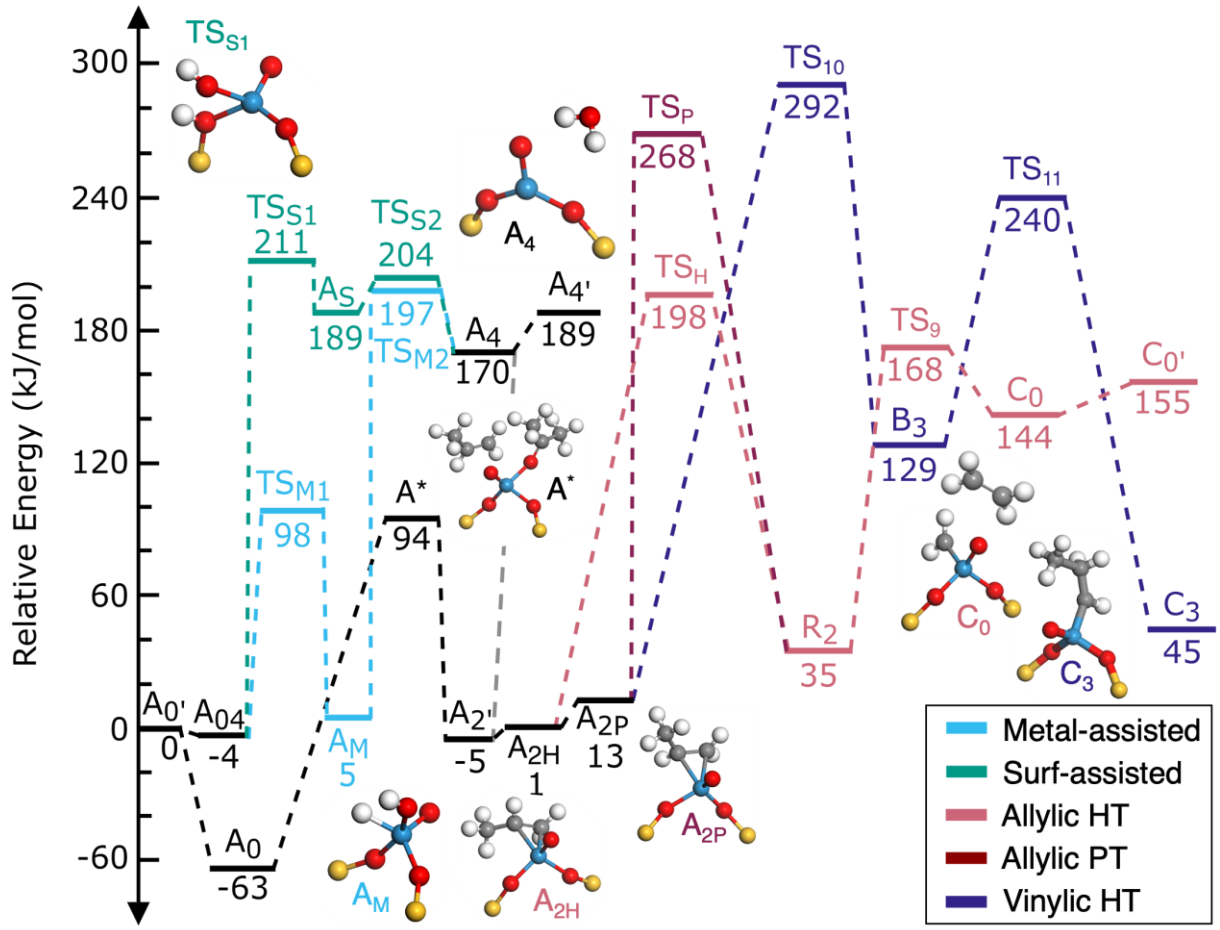

Figure 5. Energy profiles for the reduction of $(\text{-SiO})_2WO_2$ to $(\text{-SiO})_2WO$ by propene (black) and by hydrogen through metal-assisted (cyan) or surface-assisted (teal) pathways; and for the allylic hydride transfer (light pink), proton transfer (dark red), and vinylic hydride transfer (dark purple) mechanisms to produce alkylidene active sites. Primed symbols represent structures with reactants desorbed to the gas phase. **A$_{0'}$** → **A$_{04}$** represents the adsorption of H_2.

In the second possibility, the reduction is initiated by a propene molecule coordinating to the oxo ligand of $(\text{-SiO})_2WO_2$ form an acetone-coordinated complex. The coordinated acetone is very unlikely to desorb as our preliminary calculations show an energy cost in excess of 95 kJ/mol (comparable to the process of **A*** → **A$_4$**), which is consistent with previous computational studies that reported difficult acetone desorption in the overall energetics.[14,17] Rather than the sequential reaction of acetone dissociation and propene coordination, we found that a concerted ligand-exchange mechanism, in which the second propene molecule assists the desorption of acetone, reduces the energy cost for W(VI) reduction to 157

kJ/mol and directly generates the same oxometallacyclopropane, **A2**, with acetone as the oxygenate side product. Experimentally, water has been observed, among other oxygenates, in the product stream of metathesis using mass spectrometry.[20] Compared to metathesis in flow reactors, Kim at al. found that in the batch reactions of alkane metathesis, it was critical to remove these byproducts by using, for example, 4A zeolites to mitigate catalytic poisoning from strong oxygenate binding.[2]

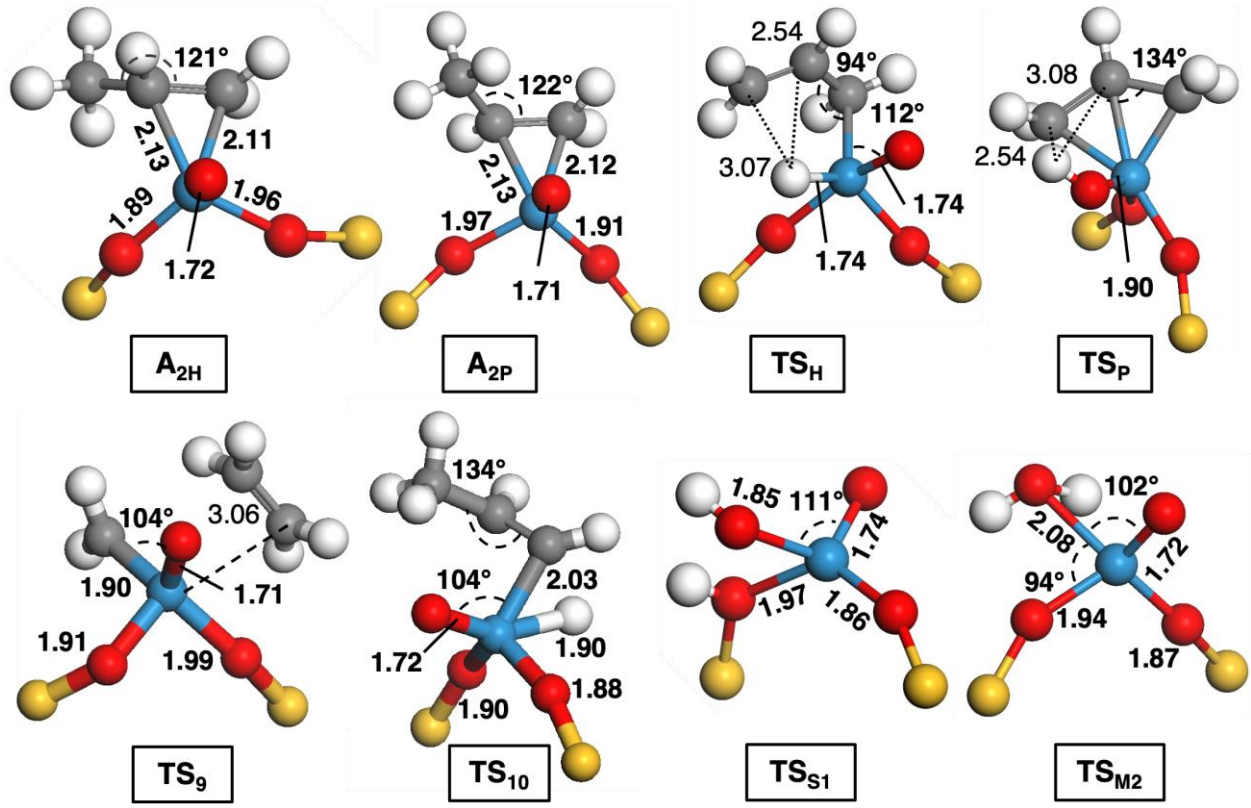

Figure 6. Optimized structures from the allylic hydride (**A2H, TSH**) and proton (**A2P, TSP**) transfer reactions, the common transition-state between both allylic reactions (**TS9**), the two transition-states from the reduction of $(\text{-SiO})_2WO_2$ by hydrogen in the metal-assisted pathway (**TSM2**) or surface-assisted pathway (**TSS1**), and the first transition state from the vinylic hydride transfer (**TS10**).

Allylic C-H activation

As mentioned earlier and shown in **Figure 5**, **A2** is the common precursor for both allylic and vinylic C-H activations. Its two stereoisomers, **A2H** and **A2P** in **Figure 6**, differ in the chirality of the center carbon atom, and correspondingly, the methyl group points away from or towards the oxo ligand, with **A2H** lower in energy than **A2P** by 12 kJ/mol. Both complexes, however, display similar structures with a slightly

extended C-C-C angle (121-122°) compared to propane and bond lengths of 2.11 – 2.13 Å for the two W-C bonds. Due to the methyl orientation, the two possible routes to activate the C-H bond are hydride and proton transfer and refer to the migration of the hydrogen atom to either the metal center or the oxygen ligand, respectively. The hydride transfer (HT) route is frequently discussed for both tungsten- and rhenium-based metathesis catalysts and produces a 14-electron, trigonal bipyramidal η^3-allyl complex (**TS$_H$**),[8,14,22] while the proton transfer (PT) route is less commonly assumed and generates a 12-electron, hydroxy complex (**TS$_P$**). In both routes, the hydrogen atom then dissociates and migrates back to the center carbon of propane, leading to a metallacyclobutane, **R$_2$**, which is a species in the metathesis cycle that can undergo [2+2] cycloreversion to generate a methylidene active site, **C$_0$**. This step has an intrinsic barrier of 133 kJ/mol, comparable to the value of 141 kJ/mol obtained for the cycloreversion of **R$_{2A}$** discussed earlier. Overall, both allylic mechanisms have rather high activation energies on this di-grafted tungsten site, with values of 261 and 331 kJ/mol for the HT and PT pathways, respectively, relative to the initial di-oxo compound **A$_0$** with two physisorbed propene molecules.

Vinylic C-H activation

Figure 5 also includes the reaction energy profile for the vinylic mechanism shown in dark purple. As with the allylic C-H activation, this mechanism starts with a coordinated propene, **A$_2$**, which undergoes α-hydrogen elimination to produce a σ-bonded metal-vinyl complex, **B$_3$**, with a high intrinsic barrier of 279 kJ/mol. Its transition state, **TS$_{10}$** in **Figure 6**, is much more distorted than the allylic counterpart **TS$_H$**. The hydride W-H bond is longer (1.90 Å) and the C-W=O angle shrinks to 104°, compared to the W-H bond of 1.74 Å and the C-W=O angle of 112° in the allylic pathway. The hydride from the vinylic complex **B$_3$** then migrates from the metal to the β carbon atom with an intrinsic barrier of 111 kJ/mol and directly leads to the formation of a propylidene active site, **C$_3$**. While the vinylic C-H activation is often mentioned as a possible mechanism in the discussions of alkylidene formation, it has not been found to be the favorable pathway with most metathesis catalysts, which is confirmed by the very high overall activation energy of 355 kJ/mol found here.

Conclusions

Propene metathesis catalyzed by silica-supported tungsten oxides was studied using ab-initio density-functional theory (DFT) calculations. The results confirmed that the heterogeneous metathesis reactions on WO_x/SiO_2 can proceed according to the Chauvin mechanism. Alkylidene carbenes function as the active species that interconvert with metallacyclobutanes through [2+2] cyclo-additions and reversions. Metallacyclobutanes are stable intermediates of a square-based pyramid geometry, and the overall potential energy barrier of 142 kJ/mol was found between the transition state for the first cycloreversion step and the metallacycle intermediate formed by the coordination of a second propene to ethylidene.

The interconversion between different forms of tungsten sites and the formation of initial alkylidene species were also investigated. It was found that on the 7-membered siloxane ring that we studied, di-grafted, di-oxo $(\text{-SiO})_2WO_2$ sites and tetra-grafted, mono-oxo $(\text{-SiO})_4WO$ sites have nearly identical energies. Starting from the dioxo precursor, the pseudo-Wittig mechanism was most favorable, with an overall energetic barrier of 193 kJ/mol, while the corresponding mono-oxo pathway is much more difficult, with an overall barrier of 323 kJ/mol. The pseudo-Wittig mechanism consists of similar [2+2] cycloaddition and reversion steps, coordinating propene to form an oxametallacycle intermediate and eliminating acetaldehyde to generate the methylidene active site directly without formal reduction to W(IV) species. By contrast, the other two active-site formation mechanisms, allylic and vinylic C-H activations, both require reduced metal centers with open coordination sites, which can be accomplished with either H_2 or reactant propene as the reductant. Propene then coordinates to form an oxometallacyclopropane. In the allylic mechanism, the methyl group undergoes C-H activation by either the metal or the oxygen ligand, with intrinsic barriers of 261 and 331 kJ/mol, respectively, to give an allyl group. Hydrogen migration to the center carbon atom then yields a metallacyclobutane, an intermediate in the main metathesis cycle. In the vinylic mechanism, a σ-bonded metal-vinyl complex was generated from the coordinated propene via α-hydrogen elimination on -CH_2 and hydrogen then migrates to the center carbon to directly form a propylidene active site. The overall energy barrier for vinylic C-H activation is 355 kJ/mol.

These findings provide plausible explanations for the experimental observations that WO_x/SiO_2 requires catalyst pretreatment at high temperatures (723 – 873 K) while the metathesis reaction itself can be operated at lower temperatures (573 – 673 K).[2,17,18] These results strongly hint at the importance of creating and maintaining alkylidenes on heterogeneous tungsten-based catalysts on metathesis activity, as reported recently.[21] It is worth noting that when pretreatment is performed separately in a reducing environment, most tungsten sites may exist in the reduced state (**A4**), leading to lower barriers for the allylic and vinylic C-H activation mechanisms. In particular, the allylic hydride transfer pathway would have an overall barrier of 197 kJ/mol. While not the focus of the present study, we note that the free-energy barrier of the pseudo-Wittig mechanism can be expected to depend more strongly on temperature than the allylic hydride transfer mechanism. Finally, this work focuses on the systematic comparison of metathesis and alkylidene formation mechanisms on the most likely tungsten site. Experimentally measured kinetic parameters will in general contain contributions from all sites, even from less likely ones if they support faster kinetics.[33,40,41] Efforts to calculate site-dependent reactivities are currently under way.

SUPPORTING INFORMATION

The following files are available free of charge: additional figures, tables, and coordinate files for key intermediates and transition states.

ACKNOWLEDGMENT

The authors are grateful for the stimulating discussions with Professor Dionisios G. Vlachos. This work was supported as part of the Center for Plastics Innovation, an Energy Frontier Research Center funded by the US Department of Energy, Office of Science, Office of Basic Energy Sciences under award number DE-SC0021166. This research used resources of the National Energy Research Scientific Computing Center (NERSC), a U.S. Department of Energy Office of Science User Facility located at Lawrence Berkeley National Laboratory, operated under Contract No. DE-AC0205CH11231 and of the Advanced Cyberinfrastructure Coordination Ecosystem (ACCESS) through allocation CTS190069, which is supported by the National Science Foundation Grant Number ACI-1548562.

REFERENCES

(1) Ellis, L. D.; Orski, S. V.; Kenlaw, G. A.; Norman, A. G.; Beers, K. L.; Román-Leshkov, Y.; Beckham, G. T. Tandem Heterogeneous Catalysis for Polyethylene Depolymerization via an Olefin-Intermediate Process. *ACS Sustain. Chem. Eng.* **2021**, *9*, 623–628. https://doi.org/10.1021/acssuschemeng.0c07612.

(2) Kim, D.; Hinton, Z. R.; Bai, P.; Korley, L. T. J.; Epps, T. H.; Lobo, R. F. Metathesis, Molecular Redistribution of Alkanes, and the Chemical Upgrading of Low-Density Polyethylene. *Appl. Catal. B* **2022**, *318*, 121873. https://doi.org/10.1016/j.apcatb.2022.121873.

(3) Chen, C.-Y.; O'Rear, D. J. Disproportionation of Alkanes via Molecular Redistribution and Molecular Averaging. *Collect. Czech. Chem. Commun.* **2008**, *73*, 1105–1111. https://doi.org/10.1135/cccc20081105.

(4) Banks, R. L.; Bailey, G. C. Olefin Disproportionation. A New Catalytic Process. *Ind. Eng. Chem. Res.* **1964**, *3*, 170–173. https://doi.org/10.1021/i360011a002.

(5) Jean-Louis Hérisson, P.; Chauvin, Y. Catalyse de Transformation Des Oléfines Par Les Complexes Du Tungstène. II. Télomérisation Des Oléfines Cycliques En Présence d'oléfines Acycliques. *Makromol. Chem.* **1971**, *141*, 161–176. https://doi.org/10.1002/macp.1971.021410112.

(6) Chauvin, Y.; Commereuc, D. Chemical Counting and Characterization of the Active Sites in the Rhenium Oxide/Alumina Metathesis Catalyst. *J. Chem. Soc., Chem. Commun.* **1992**, No. 6, 462. https://doi.org/10.1039/c39920000462.

(7) Copéret, C.; Berkson, Z. J.; Chan, K. W.; de Jesus Silva, J.; Gordon, C. P.; Pucino, M.; Zhizhko, P. A. Olefin Metathesis: What Have We Learned about Homogeneous and Heterogeneous Catalysts from Surface Organometallic Chemistry? *Chem. Sci.* **2021**, *12*, 3092–3115. https://doi.org/10.1039/D0SC06880B.

(8) Lwin, S.; Wachs, I. E. Olefin Metathesis by Supported Metal Oxide Catalysts. *ACS Catal.* **2014**, *4*, 2505–2520. https://doi.org/10.1021/cs500528h.

(9) Wachs, I. E. Progress in Catalysis by Mixed Oxides: From Confusion to Catalysis Science. *Catal. Today* **2022**. https://doi.org/10.1016/j.cattod.2022.08.025.

(10) Sautet, P.; Delbecq, F. Catalysis and Surface Organometallic Chemistry: A View from Theory and Simulations. *Chem. Rev.* **2010**, *110*, 1788–1806. https://doi.org/10.1021/cr900295b.

(11) Bouhoute, Y.; Grekov, D.; Szeto, K. C.; Merle, N.; De Mallmann, A.; Lefebvre, F.; Raffa, G.; Del Rosal, I.; Maron, L.; Gauvin, R. M.; Delevoye, L.; Taoufik, M. Accessing Realistic Models for the WO_3 –SiO_2 Industrial Catalyst through the Design of Organometallic Precursors. *ACS Catal.* **2016**, *6*, 1–18. https://doi.org/10.1021/acscatal.5b01744.

(12) Mougel, V.; Chan, K.-W.; Siddiqi, G.; Kawakita, K.; Nagae, H.; Tsurugi, H.; Mashima, K.; Safonova, O.; Copéret, C. Low Temperature Activation of Supported Metathesis Catalysts by Organosilicon Reducing Agents. *ACS Cent. Sci.* **2016**, *2*, 569–576. https://doi.org/10.1021/acscentsci.6b00176.

(13) Blanc, F.; Berthoud, R.; Coperet, C.; Lesage, A.; Emsley, L.; Singh, R.; Kreickmann, T.; Schrock, R. R. Direct Observation of Reaction Intermediates for a Well Defined Heterogeneous Alkene Metathesis Catalyst. *Proc. Natl. Acad. Sci. U.S.A.* **2008**, *105*, 12123–12127. https://doi.org/10.1073/pnas.0802147105.

(14) Handzlik, J.; Kurleto, K.; Gierada, M. Computational Insights into Active Site Formation during Alkene Metathesis over a MoO_x/SiO_2 Catalyst: The Role of Surface Silanols. *ACS Catal.* **2021**, *11*, 13575–13590. https://doi.org/10.1021/acscatal.1c03912.

(15) Kurleto, K.; Tielens, F.; Handzlik, J. Isolated Molybdenum(VI) and Tungsten(VI) Oxide Species on Partly Dehydroxylated Silica: A Computational Perspective. *J. Phys. Chem. C* **2020**, *124*, 3002–3013. https://doi.org/10.1021/acs.jpcc.9b09586.

(16) Handzlik, J. Theoretical Investigations of Isolated Mo(VI) and Mo(IV) Centers of a Molybdena−Silica Catalyst for Olefin Metathesis. *J. Phys. Chem. C* **2007**, *111*, 9337–9348. https://doi.org/10.1021/jp071568y.

(17) Howell, J. G.; Li, Y.-P.; Bell, A. T. Propene Metathesis over Supported Tungsten Oxide Catalysts: A Study of Active Site Formation. *ACS Catal.* **2016**, *6*, 7728–7738. https://doi.org/10.1021/acscatal.6b01842.

(18) Lwin, S.; Li, Y.; Frenkel, A. I.; Wachs, I. E. Nature of WO_x Sites on SiO_2 and Their Molecular Structure–Reactivity/Selectivity Relationships for Propylene Metathesis. *ACS Catal.* **2016**, *6*, 3061–3071. https://doi.org/10.1021/acscatal.6b00389.

(19) Basrur, A. Propene Metathesis over Silica-Supported Tungsten Oxide Catalyst- Catalyst Induction Mechanism. *J. Catal.* **1991**, *127*, 86–95. https://doi.org/10.1016/0021-9517(91)90211-L.

(20) Lwin, S.; Wachs, I. E. Catalyst Activation and Kinetics for Propylene Metathesis by Supported WO_x/SiO_2 Catalysts. *ACS Catal.* **2017**, *7*, 573–580. https://doi.org/10.1021/acscatal.6b03097.

(21) Gani, T. Z. H.; Berkson, Z. J.; Zhu, R.; Kang, J. H.; Di Iorio, J. R.; Chan, K. W.; Consoli, D. F.; Shaikh, S. K.; Copéret, C.; Román-Leshkov, Y. Promoting Active Site Renewal in Heterogeneous Olefin Metathesis Catalysts. *Nature* **2023**, *617*, 524–528. https://doi.org/10.1038/s41586-023-05897-w.

(22) Salameh, A.; Copéret, C.; Basset, J.-M.; Böhm, V. P. W.; Röper, M. Rhenium(VII) Oxide/Aluminum Oxide: More Experimental Evidence for an Oxametallacyclobutane Intermediate and a Pseudo-Wittig Initiation Step in Olefin Metathesis. *Adv. Synth. Catal.* **2007**, *349*, 238–242. https://doi.org/10.1002/adsc.200600440.

(23) Tielens, F.; Gervais, C.; Lambert, J. F.; Mauri, F.; Costa, D. Ab Initio Study of the Hydroxylated Surface of Amorphous Silica: A Representative Model. *Chem. Mater.* **2008**, *20*, 3336–3344. https://doi.org/10.1021/cm8001173.

(24) Kresse, G.; Furthmüller, J. Efficiency of Ab-Initio Total Energy Calculations for Metals and Semiconductors Using a Plane-Wave Basis Set. *Comput. Mater. Sci.* **1996**, *6*, 15–50. https://doi.org/10.1016/0927-0256(96)00008-0.

(25) Kresse, G.; Joubert, D. From Ultrasoft Pseudopotentials to the Projector Augmented-Wave Method. *Phys. Rev. B* **1999**, *59*, 1758–1775. https://doi.org/10.1103/PhysRevB.59.1758.

(26) Perdew, J. P.; Burke, K.; Ernzerhof, M. Generalized Gradient Approximation Made Simple. *Phys. Rev. Lett.* **1996**, *77*, 3865–3868. https://doi.org/10.1103/PhysRevLett.77.3865.

(27) Grimme, S.; Ehrlich, S.; Goerigk, L. Effect of the Damping Function in Dispersion Corrected Density Functional Theory. *J. Comput. Chem.* **2011**, *32*, 1456–1465. https://doi.org/10.1002/jcc.21759.

(28) Grimme, S.; Antony, J.; Ehrlich, S.; Krieg, H. A Consistent and Accurate Ab Initio Parametrization of Density Functional Dispersion Correction (DFT-D) for the 94 Elements H-Pu. *J. Chem. Phys.* **2010**, *132*, 154104. https://doi.org/10.1063/1.3382344.

(29) Blöchl, P. E. Projector Augmented-Wave Method. *Phys. Rev. B* **1994**, *50*, 17953–17979. https://doi.org/10.1103/PhysRevB.50.17953.

(30) Jónsson, H.; Mills, G.; Jacobsen, K. W. Nudged Elastic Band Method for Finding Minimum Energy Paths of Transitions. In *Classical and Quantum Dynamics in Condensed Phase Simulations*; WORLD SCIENTIFIC: LERICI, Villa Marigola, 1998; pp 385–404. https://doi.org/10.1142/9789812839664_0016.

(31) Henkelman, G.; Uberuaga, B. P.; Jónsson, H. A Climbing Image Nudged Elastic Band Method for Finding Saddle Points and Minimum Energy Paths. *J. Chem. Phys.* **2000**, *113*, 9901–9904. https://doi.org/10.1063/1.1329672.

(32) Vandervelden, C. A.; Khan, S. A.; Scott, S. L.; Peters, B. Site-Averaged Kinetics for Catalysts on Amorphous Supports: An Importance Learning Algorithm. *React. Chem. Eng.* **2019**, *5*, 77–86. https://doi.org/10.1039/C9RE00356H.

(33) Malviya, S.; Bai, P. Computational Investigation of Site-Dependent Activation Barriers of Zeolite-Catalyzed Protolytic Cracking Reactions. *ACS Catal.* **2023**, *13*, 179–190. https://doi.org/10.1021/acscatal.2c04192.

(34) Kiani, D.; Sourav, S.; Taifan, W.; Calatayud, M.; Tielens, F.; Wachs, I. E.; Baltrusaitis, J. Existence and Properties of Isolated Catalytic Sites on the Surface of β-Cristobalite-Supported, Doped Tungsten Oxide Catalysts (WO_x/β-SiO_2, Na-WO_x/β-SiO_2, Mn-WO_x/β-SiO_2) for Oxidative Coupling of Methane (OCM): A Combined Periodic DFT and Experimental Study. *ACS Catal.* **2020**, *10*, 4580–4592. https://doi.org/10.1021/acscatal.9b05591.

(35) Guesmi, H.; Grybos, R.; Handzlik, J.; Tielens, F. Characterization of Tungsten Monomeric Oxide Species Supported on Hydroxylated Silica; a DFT Study. *RSC Adv.* **2016**, *6*, 39424–39432. https://doi.org/10.1039/C6RA05395E.

(36) Kroenlein, K.; Muzny, C. D.; Kazakov, A. F.; Diky, V.; Chirico, R. D.; Magee, J. W.; Abdulagatov, I.; Frenkel, M. "NIST Standard Reference Database 203: TRC Web Thermo Tables (WTT) Version 2-2012-1 Professional", National Institute of Standards and Technology, Gaithersburg MD, 20899. https://wtt-pro.nist.gov/ (accessed 2023-03-19).

(37) Begley, J. The Kinetics of Propylene Disproportionation. *J. Catal.* **1967**, *9*, 375–395. https://doi.org/10.1016/0021-9517(67)90265-5.

(38) Mougel, V.; Santiago, C. B.; Zhizhko, P. A.; Bess, E. N.; Varga, J.; Frater, G.; Sigman, M. S.; Copéret, C. Quantitatively Analyzing Metathesis Catalyst Activity and Structural Features in Silica-Supported Tungsten Imido–Alkylidene Complexes. *J. Am. Chem. Soc.* **2015**, *137*, 6699–6704. https://doi.org/10.1021/jacs.5b03344.

(39) Solans-Monfort, X.; Copéret, C.; Eisenstein, O. Metallacyclobutanes from Schrock-Type d^0 Metal Alkylidene Catalysts: Structural Preferences and Consequences in Alkene Metathesis. *Organometallics* **2015**, *34*, 1668–1680. https://doi.org/10.1021/acs.organomet.5b00147.

(40) Goldsmith, B.; Sanderson, E.; Bean, D.; Peters, B. Isolated Catalyst Sites on Amorphous Supports: A Systematic Algorithm for Understanding Heterogeneities in Structure and Reactivity. *The Journal of chemical physics* **2013**, *138*, 204105. https://doi.org/10.1063/1.4807384.

(41) Khan, S. A.; Godahewa, S. M.; Wimalasiri, P. N.; Thompson, W. H.; Scott, S. L.; Peters, B. Modeling the Structural Heterogeneity of Vicinal Silanols and Its Effects on $TiCl_4$ Grafting onto Amorphous Silica. *Chem. Mater.* **2022**, *34*, 3920–3930. https://doi.org/10.1021/acs.chemmater.1c04016.